Effect of processing parameters on the morphology development during extrusion of polyethylene tape: an in-line Small-Angle X-ray Scattering (SAXS) study

Journal Item

Effect of processing parameters on the morphology development during extrusion of polyethylene tape: An in-line Small-Angle X-ray Scattering (SAXS) study

E.L. Heeley, [a]* T. Gough,[b] D.J. Hughes,[c] W. Bras,[d] J. Rieger,[e] A.J. Ryan[f].

[a]Department of Physical Sciences, Open University, Walton Hall, Milton Keynes, MK7 6AA, UK.
[b]School of Engineering, Design and Technology, University of Bradford, Bradford, BD7 1DP, UK.
[c]WMG, University of Warwick, Coventry, CV4 7AL, UK.
[d]Netherlands Organization for Scientific Research (NWO), DUBBLE-CRG / ESRF, B.P. 220, F-38043 Grenoble Cedex, France.
[e]BASF SE, Polymer Physics, 67056 Ludwigshafen, Germany.
[f]The Polymer Centre, Department of Chemistry, University of Sheffield, Sheffield, S3 7HF, UK.

*Corresponding author: E.L. Heeley; Ellen.Heeley@open.ac.uk; +44(0)1908 655194.

Keywords: polymer extrusion, low density polyethylene (LDPE); Small-Angle X-Ray scattering (SAXS).

Abstract

The in-line development of crystalline morphology and orientation during melt extrusion of low density polyethylene (LDPE) tape at nil and low haul-off speeds has been investigated using Small-Angle X-Ray Scattering (SAXS). The processing parameters, namely haul-off speed and distance down the tape-line have been varied and the resulting crystalline morphology is described from detailed analysis of the SAXS data. Increasing haul-off speed increased orientation in the polymer tape and the resulting morphology could be described in terms of regular lamellar stacking perpendicular to the elongation direction. In contrast, under nil haul-off conditions the tape still showed some orientation down the tape-line, but a shish-kebab structure prevails. The final lamellae thickness (~50 Å) and bulk crystallinity (~20%), were low for all processing conditions investigated, which is attributed to the significant short-chain branching in the polymer acting as point defects limiting lamellae crystal growth.

1. Introduction

Although the industrial extrusion of polyolefins in fibre and tape form is widely applied, there is an interdependence of processing parameters on the finally crystalline morphology which is not fully understood [1]. The flow and thermal history of the material affects the crystallization kinetics and morphology and knowledge of the nature of these dependencies is required for consistent industrial processing. Once manufactured, the polymer morphology is stabilised by the crystallization process. The type of nucleation and subsequent crystallization is profoundly influenced by flow due to the alignment or orientation of the molecular chains [2-5]. The route to crystallization during flow is generally accepted to be via the formation of 'shish-kebab' morphology [6-9]. Proposed mechanisms and kinetics for the formation of shish-kebab morphology usually relate to data from shear flow conditions using custom made shearing devices [10-16]. However, during extrusion, the polymer melt exits the die head and begins to cool rapidly, and at the same time it is uniaxially elongated under constant force, between the die head and take-up device. This imposes a high extensional flow on the tape or fibre in the drawing line which, in turn, influences the crystallization kinetics and morphology when compared with shear flow conditions. This is due to the stress imposed, take-up velocity and non-isothermal cooling process.

Following the orientation and crystallization development in polymer tapes and fibres during processing, requires real-time measurements and several techniques can be employed to do this. A recent review by Alig [17] of monitoring polymer melt processing, details *off-line* and *in-line* measurements; the latter being the most useful in following real-time morphology development. In-line monitoring techniques should provide data that is of sufficient time resolution and quality to be of quantitative use. Spectroscopic, ultrasonic and X-ray scattering techniques have proven invaluable to monitor structure development, composition and material properties during processing [17-22].

Recently, several works have investigated the orientation and shish-kebab (or microfibrillar) structure development under extensional flow conditions after

processing, using X-ray and microscopy techniques. Rybnikar [23] focused on using controlled temperature and high pressure extrusion of high density polyethylene (HDPE) tapes. Low orientation produced tapes with a slightly deformed spherulitic structure whereas highly oriented tapes possessed a shish-kebab structure containing voids and cracks from the lateral coherence of parallel fibrils. Zheng [24] detailed the extrusion with contiguous stretching of polypropylene (PP) films. Subsequent annealing and recrystallization of the off-line samples gave denser and shorter oriented shish-kebab structures at high stretching rates, compared with dense but longer structures at low stretching rates. Murase [25] gave a comprehensive study of the flow-induced self-assembling structures that evolve down a fibre spin-line for concentrated polymer solutions proposing a two-stage pathway for shish-kebab formation. Early stages saw the evolution of transient phases leading to string-like structures. Later stages were dominated by flow-induced bundles of stretched chains resulting in shish-kebab structures. Polaskova [26] reported on the formation of the microfibrillar-phase structure of PE/PP blends where the orientation increased with the increasing amount of PP in the bend. The blends were easier to process having improved mechanical properties compared to the hompolymers. Finally, Chen [27] described the precursor morphology formed in polyester fibres consisting of highly oriented molecular chains. These can be problematic in the melt-spinning processing by reducing chain mobility and hence interrupting molecular orientation, limiting the final fibre properties.

Several studies have monitored the *in-line* structure development during polymer processing. Cakmak [21] followed the structure development in melt spun poly(vinylidene fluoride) PVDF tape, using combined small- and wide-angle X-ray scattering (SAXS/WAXS) and Hirahata [28] studied poly(ethylene terephthalate) PET using WAXS. Both observed that increasing the haul-off speed of the fibre increased the orientation and lamellar repeat distances, thus the morphology changed from spherulitic to a sheaf-like structures. Further to this, earlier publications by the authors [29-31] have detailed SAXS/WAXS studies on extrusion of polypropylene tapes, which concentrated on observing the onset of large-scale ordering prior to any crystalline growth. The onset was revealed by the development of intensity in the SAXS data before crystalline peaks in the WAXS data are observed. Later insights

have made it clear that this is intrinsic to the experiment and related to the sensitivity of the different techniques [32,33]. Other groups have also seen similar results when investigating the early stages of the fibre melt spinning process. Samon *et al* [34-38] have reported on the crystalline development in melt spinning of several polymers (nylon 6, PE, PVDF and poly(oxymethylene) (POM)) again using SAXS/WAXS as a function of distance and take-up speed from the spinneret. Equatorial SAXS scattering was seen to develop before the meridional SAXS patterns, which was interpreted as indicating the initial stages of shish-kebab or microfibril crystallization. Kolb [39] also studied melt spinning of PP fibres as a function of take-up speed and spinneret height observing the growth of oriented crystals from an unoriented amorphous matrix. All of these investigations reported a flow-induced shish-kebab type of morphology in the final fibre.

In this study we focus on the morphology development in low density polyethylene (LDPE) tapes at nil and low haul-off speeds (being considerably less than those used during the melt spinning of fibres). Previous works have only detailed investigations on high density PE (HDPE) fibres [34,36,37]. Here, in-line SAXS was used to monitor the crystallinity, orientation and structure development of the LDPE tape with respect to varying processing parameters: haul-off speed and distance down the tape-line. The elongation of the extruded tape was controlled by employing a Rheotens instrument [40] which also allows the draw-down force to be measured enabling the direct evaluation of stress experienced by the tape. This removes the need for take-up rolls where the tape is constantly wound-up, which can change the draw-down speed during the SAXS data acquisition. Hence, this added experimental uncertainty is eliminated. A comprehensive data set is presented allowing a parametric profile of crystalline structure, crystallinity and orientation with haul-off speed and distance down the tape-line.

2. Experimental

2.1 Material

A low density commercial grade polyethylene, Lupolen 1840H GPC M_w = 250 000 g/mol, M_w/M_n = 13.5, MFI (190 °C) = 1.5 g/10 min, T_m (DSC) ≈112 °C, provided by

BASF, was used for all extrusion experiments. Lupolen 1840H has a significant amount of short-chain (30 CH_3/1000 C) and long-chain branching [41].

2.2 Extruder instrumentation

An AXON BX18 single screw lab-scale extruder with 18 mm diameter screw was positioned above the X-ray beam on a horizontal, height-adjustable platform as shown in Figure 1. The distance between the die head and X-ray position was varied between 760 mm and 1600 mm. The extruder barrel temperature profile was determined by six zones: the feed zone 1, at 140 °C; zone 2 at 145 ^{o}C; zones 3-5 at 150 °C and die head zone 6, at 150 °C. The extruder screw speed was set at 3.0 Hz giving a mass flow rate of 5.06 g/min. The polymer tape was extruded from the die head (dimensions 3 mm × 0.5 mm) and fed by guides to the X-ray position. The tape cooled rapidly after exiting the die head. The ambient air temperature was controlled at 20 °C in the experimental zone. The tape temperature was recorded at the X-ray position by locating a K-type thermocouple against the tape. The thermocouple was pressed into the tape until a steady temperature was obtained. Although, this method only measured the skin temperature of the tape, it did allow comparisons between data sets to be recorded as reliably as practicable.

A Göttfert Rheotens[40] instrument was situated below the X-ray position to provide a constant haul-off speed on the extruded tape for each experiment. The haul-off speeds were varied at each chosen height between 3.0 and 50.4 m/min. The force applied to the tape was measured by a force balance in the arm onto which the haul-off wheels were attached. The force balance was calibrated using defined weights. Off-line samples of the tape were taken for each run and the dimensions measured using a micrometer (width and thickness) giving the cross-sectional area at the X-ray position. Hence, the stress experienced by the tape at the X-ray position was determined. The applied stress was calculated at each height and haul-off speed. As to be expected the increasing haul-off speed increases the stress in the tape in a linear fashion at all heights (see Figure S1 in supplementary data for plot).

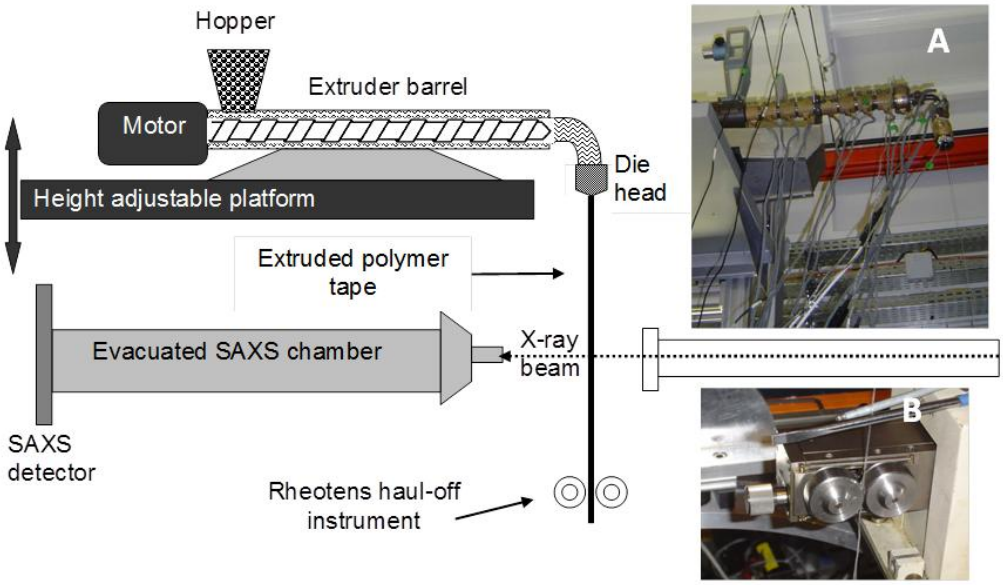

Figure 1. Extruder set-up on the X-ray beamine. Inset pictures show (A) extruder barrel and die head positioned on a height-adjustable platform and (B) details of the Rheotens instrument.

2.3 X-ray scattering measurements and data analysis

Real-time SAXS data measurements down the tape-line were performed on the DUBBLE BM26 beamline at the ESRF in Grenoble, France. The DUBBLE beamline optics and construction are detailed elsewhere [32]. An X-ray wavelength, λ, of 1.24 Å was used for all measurements. SAXS data were collected using a (2D) gas-filled multiwire area detector situated 6 m from the sample position (an evacuated chamber was positioned between the sample and the detector to reduce air scattering and absorption). The data was corrected for background scattering from the experimental set-up, sample thickness and transmission (via two parallel-plate ionization chambers positioned before and after the sample) and any detector spatial distortion. An oriented specimen of wet rat-tail collagen was used to calibrate the SAXS detector.

The tape extrusion is a steady-state process, thus the distance down the tape-line at the point of observation correlates with the time elapsed since the material left the die head. Hence, the polymer material at the point of the X-ray beam is continuously replaced with material having identical extensional and temperature history. The SAXS data was collected at a rate of 20 seconds per frame. The 2D SAXS data were reduced to 1D profiles of intensity (I) versus scattering vector (q), where $q = (4\pi \sin$

θ/λ) and θ is the scattering angle. This was achieved by performing a sector integration on the meridional scattering pattern using a fixed radius and integration angle with the CCP13 BSL software [15,42]. The integration plots were then analysed using purpose written correlation function software known as Corfunc [15,42,43]. The correlation function is expressed as:

$$\gamma_1(R) = \frac{1}{Q_s}\int_0^\infty I(q)q^2\cos(qR)\mathrm{d}q \qquad (1)$$

where *I(q)* is the scattering intensity and the relative invariant Q_s,is defined as:

$$Q_s(t) = \int_0^\infty q^2 I(q)\mathrm{d}q \approx \int_{q_1}^{q_2} q^2 I(q)\mathrm{d}q \qquad (2)$$

The invariant Q_s, is obtained from the integration of the 1D SAXS curve between accessible experimental limits of $q = q_1$ which is the first reliable data point and $q = q_2$, taken from the region of the curve where $I(q)$ is constant. Here, Q_s, depends upon the volume fraction of crystallites but may also be affected by the volume of material at the X-ray point. In this case, the decrease in tape volume would decrease Q_s, however it is only a scaling factor in the correlation function and other authors [34, 38] assume that any reduction is small. Thus generally, an increase in Q_s correlates to an increase in scattering from the crystallization in the polymer tape.

Calculating and interpreting the correlation function involves the extrapolation and integration of the non-Lorentz corrected 1D SAXS data. The data were extrapolated to $q \to \infty$ according to Porod's law [44], $I \sim q^{-4}$, and to $q \to 0$ according to the Guinier model [45], $I \sim A + Bq^2$. The correlation function analysis interprets the parameters with respect to an ideal two-phase lamellar microstructure model [45-48]. The correlation function analysis allowed various parameters to be extracted from the data such as long period (L_p), crystalline and amorphous layer thicknesses (H_b and S_b respectively) and an estimated bulk volume crystallinity.

Finally, the SAXS data was analysed to obtain an estimate of the relative orientation. The 2D SAXS patterns were reduced to 1D plots where the angular variation in intensity, $I(q^*, \phi)$, was obtained at a fixed radius q^* over an azimuthal angle, ϕ, range

of 0–360°. The full width half-maximum (FWHM) for the two meridional peaks were fitted using a Lorentzian function and averaged.

3. Results and discussion

3.1 Measurement of tape temperature and cross-sectional area

The temperature and cross-sectional area of the tape at the X-ray position with respect to increasing haul-off speed at each height are shown in Figure 2A and 2B respectively.

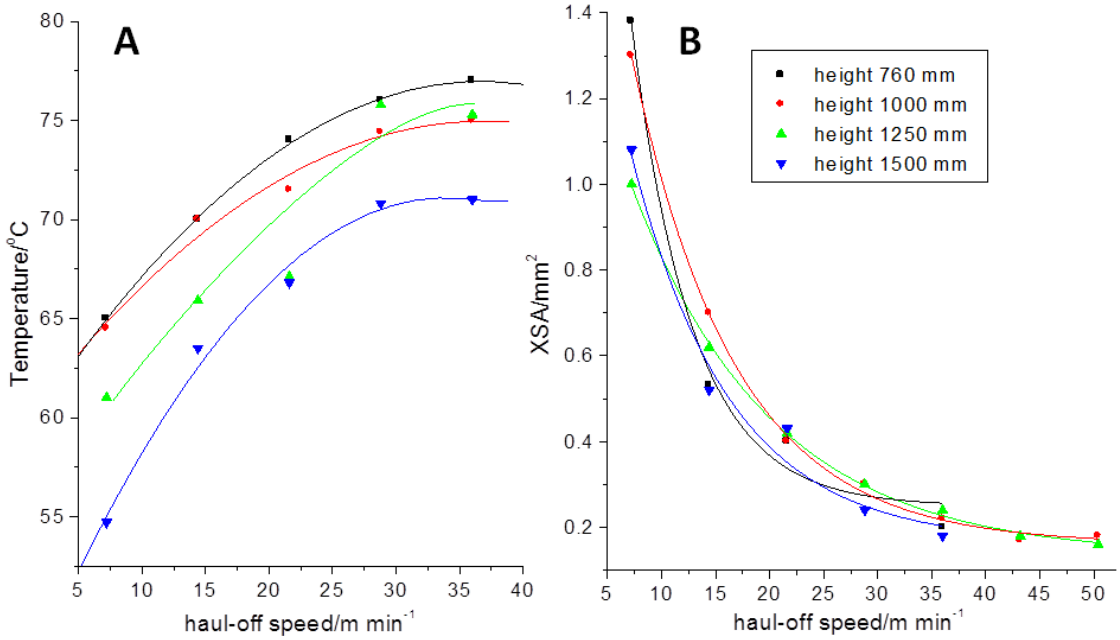

Figure 2. (**A**): Graph of tape temperature versus haul-off speed with increasing height and (**B**): change in tape cross-sectional area (XSA) versus haul-off speed with increasing height.

At constant height, the temperature of the tape at the X-ray point increases as the haul-off speed increases, that is, as the polymer moves down the tape-line faster it will have less time to cool when reaching the X-ray point. At a constant haul-off speed the tape temperature decreases with increasing height; the polymer travels further down the tape-line having more time at ambient temperature to cool. It is possible to link the temperature of the tape to its cross-sectional area (Figure 7B). Clearly, as the haul-off speed increases the cross-sectional area decreases, that is, the tape will become thinner as the draw ratio increases. Thinner tapes cool faster, however, the temperature of the tape starts to plateau above haul-off speeds of ~28 m/min at all

heights, this is mirrored by the change of cross-sectional area where a plateau also occurs at all heights above this haul-off speed.

3.2 Qualitative analysis of 2D SAXS data

Figure 3, shows a matrix of 2D SAXS patterns measured at various distances down the tape-line with increasing haul-off speed (the central spot in all patterns is the X-ray beam stop). The direction of the tape-line elongation is vertical in all the SAXS patterns. At a low haul-off speed of 7.2 m/min, the SAXS patterns change from an unoriented halo at a height of 760 mm to an oriented pattern with two distinct lobes on the meridian (parallel to tape-line) at a height of 1500 mm. However, there is still some obvious scattering which occurs radially in the pattern. In contrast, increasing the haul-off speed to 36 m/min, at a height of 760 mm, we observe an oriented two-lobed weak SAXS pattern, which increases in intensity and definition as the height is increased. Finally, at 1500 mm a highly oriented 'tear-drop' pattern is observed without any additional radial scattering. The SAXS patterns can be interpreted in terms of a two-phase lamellar system where the lamellae stacks are perpendicular to the tape elongation direction, as has previously been reported for polyolefins when crystallized from oriented melts during shear and melt-spinning processes [9,15,34,36,49,50].

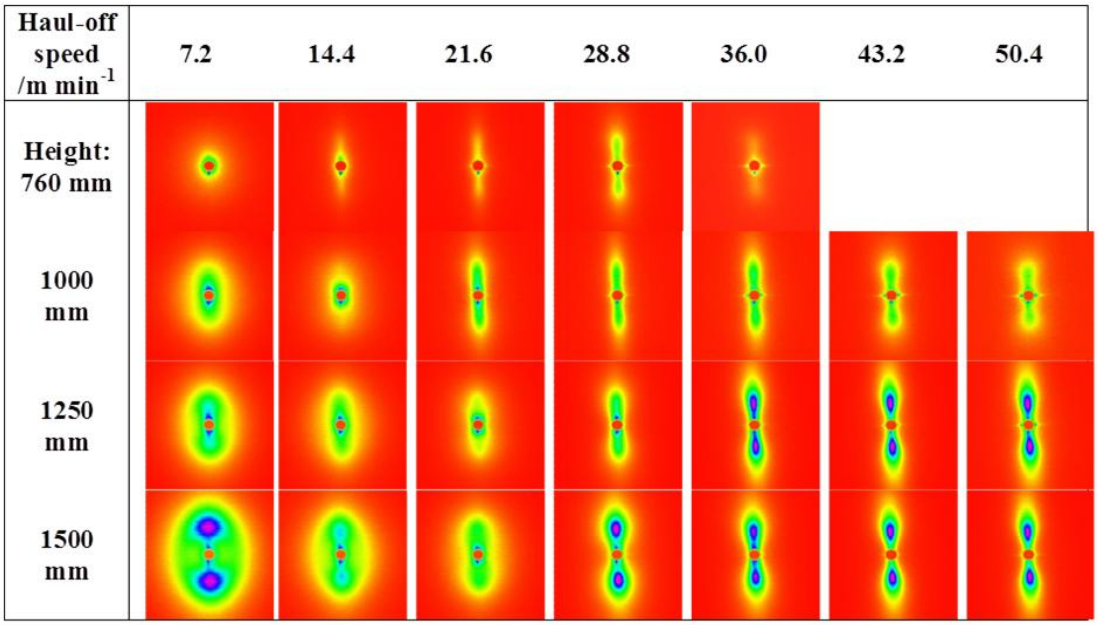

Figure 3. Matrix of 2D SAXS patterns of LDPE tape at various heights and haul-off speeds with a mass flow rate of 5.06 g/min and die temperature 150 °C.

To interpret the different structures seen in the 2D SAXS we refer to Figure 4, which shows the tear-drop SAXS shape (A), representing a stack of parallel lamellae where there is a distribution of crystal lamellae and amorphous thicknesses. Here, the lobes in the SAXS patterns are broadened in the meridional direction (towards the beamstop) due to the irregular thicknesses and distances between lamellae. As the lamellae become more regularly spaced and of equal thickness the SAXS lobes become sharp as in (B), giving a distinct two spot pattern. Finally in (C), the arced SAXS pattern indicates narrow lamellae or shish-kebab structures with varying orientations deviating from the vertical elongation direction [51]. It should be noted that these are general representations of SAXS patterns and their associated morphology and thus, from the SAXS patterns observed here, there is likely to be a mixture of the structures present. For example, at a haul-off speed of 7.2 m/min and a height of 1500 mm a combination of regular stacked lamellae (presented as sharp meridional lobes) and the radial scattering indicates a presence narrow lamellae with various orientations around the tape axis. At higher haul-off speeds and heights the SAXS patterns transform to a distinct two spot shape where tape consists of highly oriented regular sized lamellae stacks.

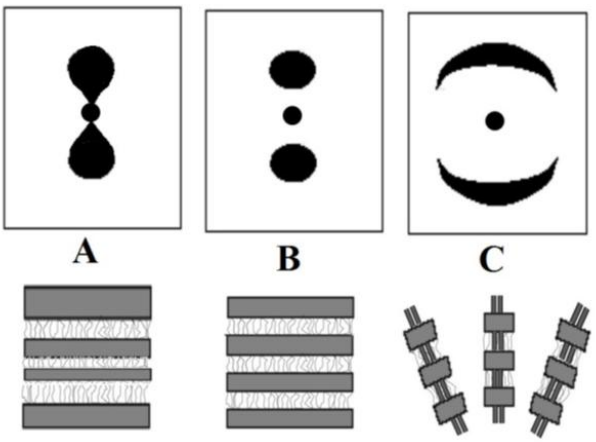

Figure 4. Schematic representation of the 2D SAXS patterns commonly observed for oriented polymer samples: (A) tear-drop shaped meridional lobes from irregular thicknesses and distances of lamellae and amorphous regions; (B) sharp meridional spots from regularly spaced lamellae; (C) meridional arcs from thin lamellae or ‘shish-kebab’ structures with many orientations.

It should be mentioned that some of the 2D SAXS patterns in Figure 3, also show evidence of scattering perpendicular to the elongation direction in the form of equatorial streaks. These are present at the same time as the meridional scattering and have been observed previously during melt spinning and shearing of polymers [36,39,49,52]. The occurrence of equatorial streaks is attributed to the formation of bundles of highly oriented molecular chains (or shish), which have a repeat distance perpendicular to the elongation direction. The 2D SAXS data in Figure 3, shows noticeable equatorial streaks at a die height of 1000 mm with haul-off speeds between 28.8 –50.4 m/min (see Figure S2 in supplementary data for extraction of 2D and 1D SAXS peaks from the equatorial region). Further to this, at haul-off speeds ≥ 36.0 m/min at heights of 1250 mm and 1500 mm some evidence of equatorial streaks are also seen, but certainly not as pronounced as those at heights of 760 – 1000 mm. At haul-off speeds ≥ 28.8 m/min as the material travels down the tape-line (increasing height) the equatorial streaks tend to diminish and the intensity of the meridional scattering increases. Here, highly oriented molecular chains or 'bundles of shish' are formed as precursors to the growth of crystallites, acting as nucleation points. It is expected that these shish are consumed in the formation of crystallites, which in turn fuse forming lamellae stacks down the tape-line [34,36]. In contrast, the SAXS data at haul-off speeds below ~28 m/min are lacking in any discernible equatorial streaks. If shish are present they would probably have a low number density and therefore do not scatter sufficiently to be observed.

To complete the discussion of the SAXS data, Figure 5 shows a series of 2D SAXS patterns of the tape with zero haul-off speed, that is, the tape was free to extrude downwards under its own weight. It is apparent from the SAXS, that a shish-kebab structure (as shown in Figure 4 C) is formed gradually down the tape-line. The SAXS pattern at 1600 mm contains significant orientation about the meridian where the scattering manifests in an arc shape. However, at heights below 1000 mm the SAXS shows a halo of intensity, indicating that the crystalline structure developing has no preferred orientation at this point. The oriented shish-kebab structure which develops as the height increases is likely to be caused by the nature of the actual extrusion process and elongation itself (under the tape's own weight) in this case. There are enough oriented shish present which should act as nucleation points for lamellae to

grow perpendicular to these shish. However, no equatorial streaks are seen in the SAXS patterns (Figure 5) at any height when the haul-off speed of the tape is zero. This indicates that even though shish prevail, they are not in significant concentrations to cause any regular scattering intensity perpendicular to the tape-line.

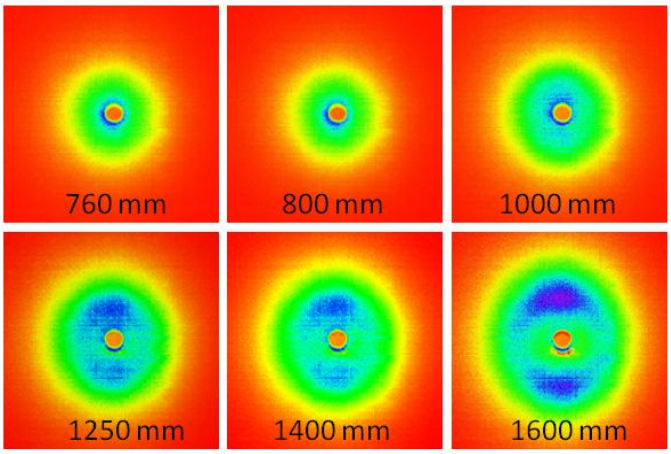

Figure 5. A series of 2D SAXS patterns down the tape-line with zero haul-off at various heights.

3.3 Quantitative analysis of orientation from SAXS

The 2D SAXS data presented in Figures 3 and 5, indicate qualitatively that the crystalline morphology of the tape has preferred orientation along the elongation direction, which increases as the haul-off speed is increased. Thus, to gain a quantitative insight into the variation in the orientation of the lamellar stacks with haul-off speed and height along the tape-line, the average FWHM of each 1D azimuthal SAXS profile was determined as described in Section 2.3. Figure 6, shows an example of a plot of fitted SAXS data over an angular range of 0–360° for the tape at a haul-off speed of 50.4 m/min and a height of 1250 mm.

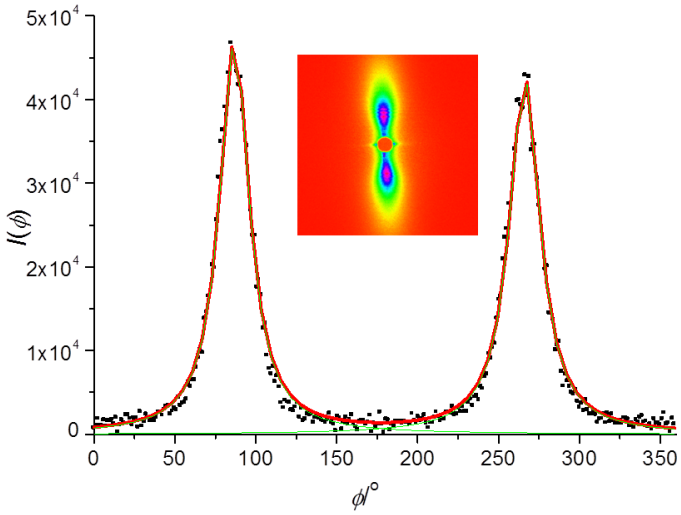

Figure 6. Example of SAXS data peaks fitted with Lorentzian functions to obtain the FWHM. Inset shows the original 2D SAXS pattern of the tape at a haul-off speed of 50.4 m/min and a height of 1250 mm.

Figure 7A, shows a series of azimuthal scans from SAXS data at a constant height of 1500 mm with varying haul-off speed. The widths of the two peaks decrease as haul-off speed increases indicating an increase in orientation of the lamellae in the direction of elongation down the tape-line. At a haul-off speed of ≥28.8 m/min the peak widths start to decrease to a lesser extent with the increase in haul-off speed. This feature is emphasised in Figure 7B, which gives an overall view of the relationship between the orientation of the lamellae down the tape-line with increasing haul-off speed.

In Figure 7B at haul-off speeds <28 m/min, the orientation increases (FWHM decreases) steadily. However, at haul-off speeds >28 m/min the orientation of the lamellae only increases slightly at each height and with little variation as haul-off speed continues to increase. That is, at higher haul-off speeds the orientation of lamellae stacks tends towards a maximum constant value at all heights. This supports the variation in the tape cross-sectional area (Figure 2B), which shows a similar trend beyond a haul-off speed of ~28 m/min.

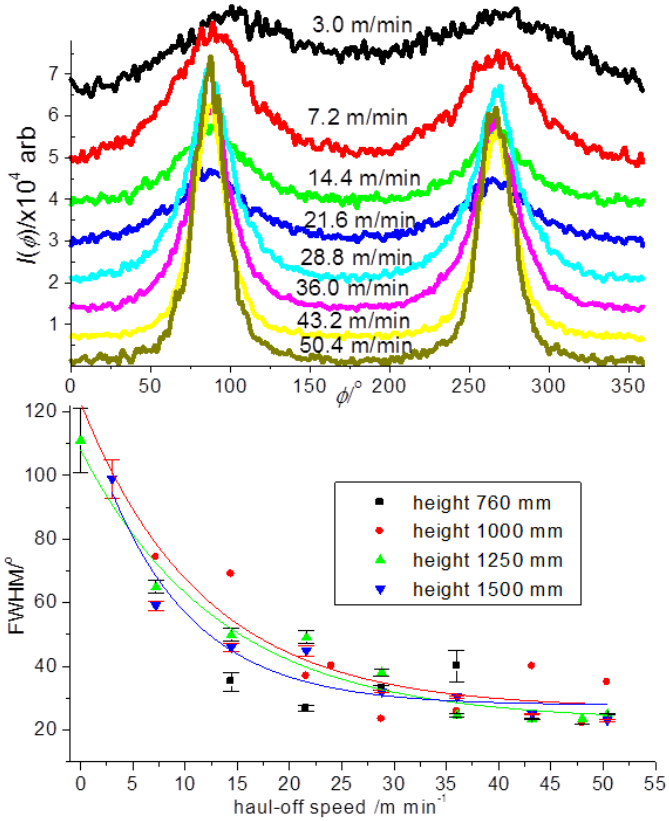

Figure 7. (**A**): Azimuthal scans from SAXS data at a constant height of 1500 mm with varying haul-off speeds (scans are off-set on the vertical axis for clarity). (**B**): Change in FWHM versus haul-off speed determined at various distances down the tape-line.

In contrast, the 1D azimuthal SAXS profiles for the tape with zero haul-off speed are given in Figure 8. From a height of 1250 mm the orientation is apparent and increases with height thereon. However, the breadth of the peaks indicates a wide variation of orientations of the lamellae parallel to the tape-line. This is further highlighted by the significant arcing in the meridional intensity observed in the associated 2D SAXS patterns (Figure 5).

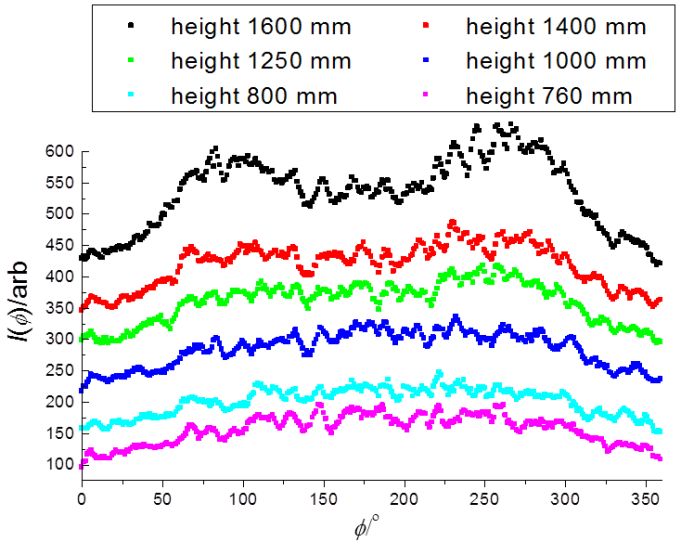

Figure 8. 1D azimuthal SAXS profiles down the tape-line with zero haul-off speed.

3.4 Correlation function analysis of the SAXS data

Correlation functions were generated from the sector integrated 2D SAXS data as described earlier (Section 2.3) which provide quantitative information on the dimensions of the lamellar stacking and bulk crystallinity down the tape-line. Figure 9A, shows an example of a 1D SAXS curve of the tape at a height of 1500 mm and a haul-off speed of 7.2 m/min with its correlation function. From the correlation function various parameters were extracted (as indicated in Figure 9B); the long period (L_p) which is the average crystalline plus amorphous layer stack distance; the crystalline layer thickness or hard block, (H_b) and thickness of the amorphous layer or soft block, (S_b) and bulk crystallinity.

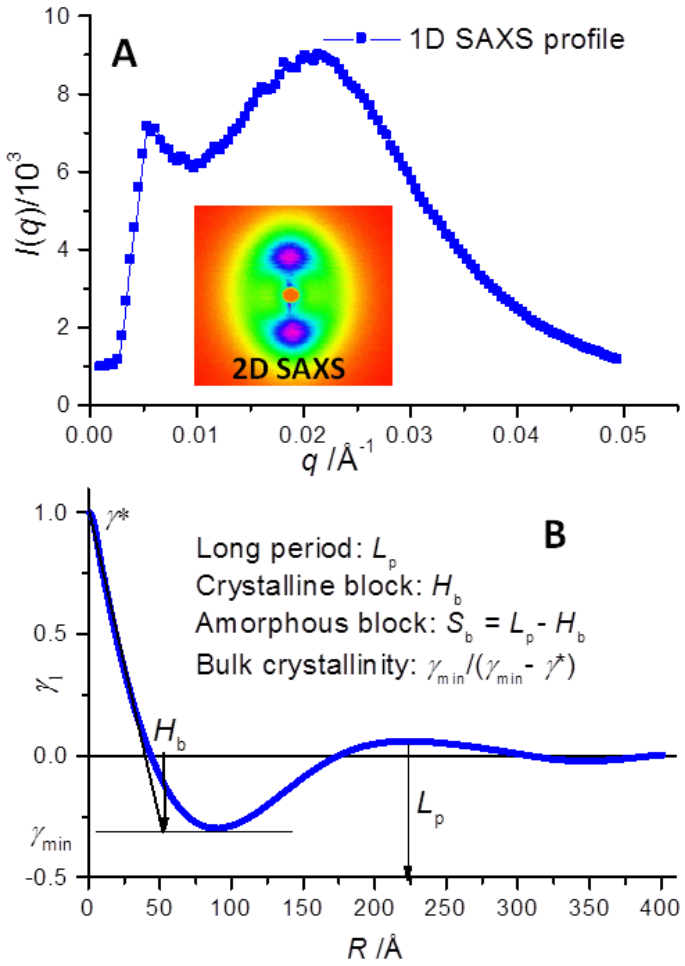

Figure 9. Example of a SAXS pattern and corresponding correlation function analysis of the tape at a height of 1500 mm and a haul-off speed of 7.2 m/min. (**A)**: The 1D SAXS profile from the 2D SAXS pattern (inset). (**B)**: Corresponding correlation function and interpretation of its features with respect to an ideal two-phase lamellar structure.

Figure 10, shows individual graphs of the parameters extracted from the correlation function analysis. From graph A, as the haul-off speed increases L_p generally increases, until a haul-off speed of ~28 m/min. After this L_p is has a relatively constant value at all heights. Again, this correlates with the orientation and cross-sectional area beginning to plateau from this haul-off speed. At lower haul-off speeds (below 28 m/min) L_p decreases down the tape-line; here the tape temperature (Figure 2A) is lower and so has had a greater amount of time to crystallize when reaching the X-ray point. The reduction of L_p is due to the insertion of lamellae into the amorphous regions and their subsequent thickening.

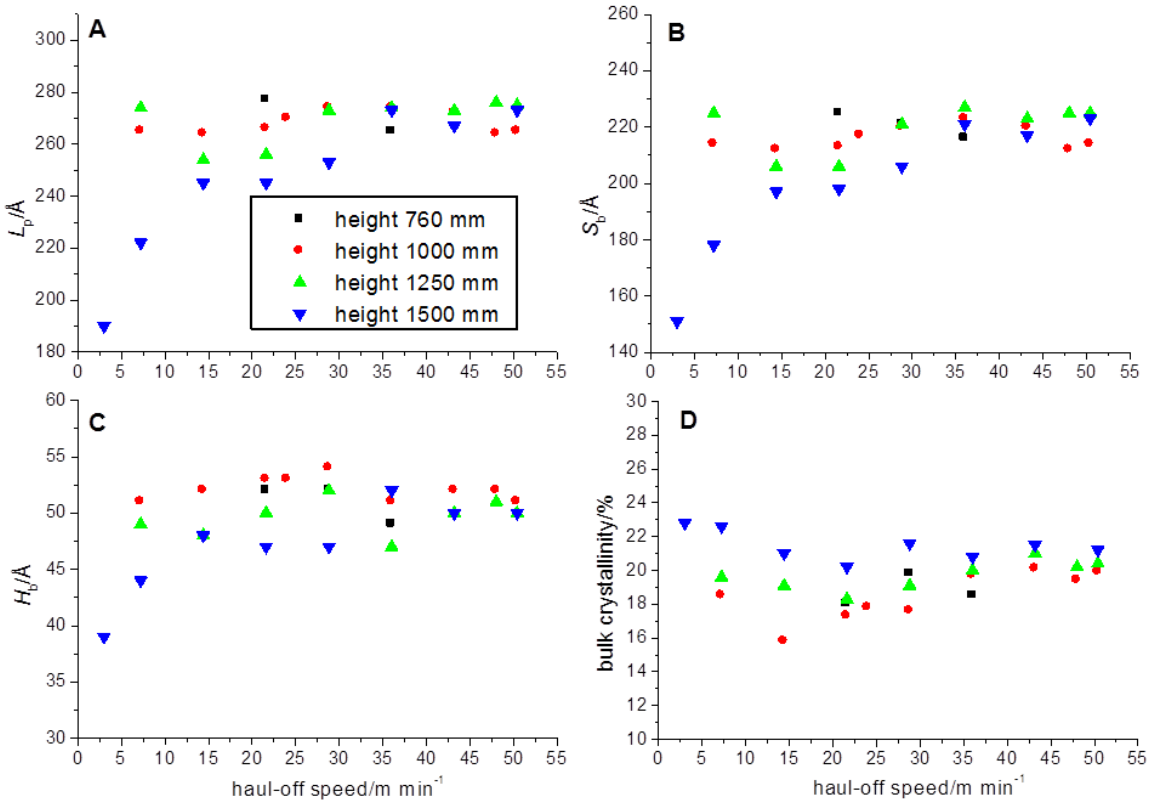

Figure 10. Change in (A) long period (L_p); (B) soft block thickness (S_b); (C) hard block (H_b) thickness and (D) bulk crystallinity down the tape-line with respect to increasing haul-off speed.

The L_p is made up of the crystalline (H_b) and amorphous regions (S_b) and any changes in L_p are therefore influenced by both these regions. Graphs B and C in Figure 10, show the changes in S_b and H_b respectively with increasing haul-off speed. The change in S_b follows a similar trend as that of the L_p. As mentioned, the reduction in L_p occurs due to the insertion and thickening of lamellae in the amorphous regions which is illustrated schematically in Figure 11. Here, the 2D SAXS patterns and corresponding reduction in L_p (lamellae and amorphous stacking) down the tape-line is given for a haul-off speed of 28.8 m/min. The 2D SAXS patterns change from a tear-drop shape with an L_p of 273 Å, to a two spot pattern where L_p is reduced to 253 Å, indicating a move from lamellae with irregular thicknesses and spacings to more regular spaced lamellae with equal thicknesses.

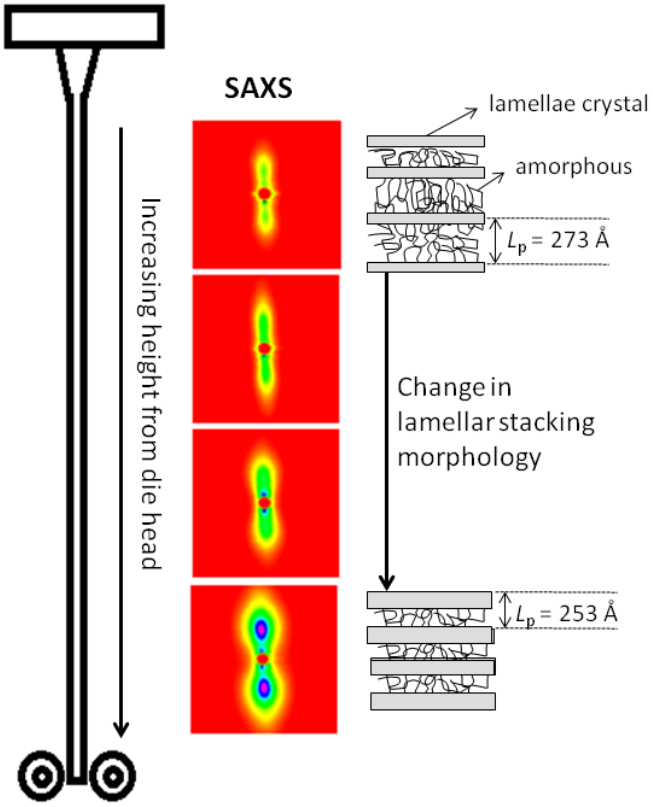

Figure 11. Change in 2D SAXS patterns and corresponding lamellar structure down the tape-line at a haul-off speed of 28.8 m/min.

One feature that is interesting from the correlation function analysis is the overall change in H_b, the crystalline layer thickness. This is seen to only increase slightly with haul-off speed ≥ 15 m/min and has a value is in the region of 45–55 Å. There is little change in the H_b thickness with respect to height either. However, the amorphous layer thickness (S_b) increases with increasing haul-off speed (until ~28 m/min) in the same fashion as the L_p, which can be attributed to increased stretching and orientation of the amorphous polymer chains. The observation that the crystalline thickness remains relatively constant at about 50 Å is a feature that has been noted before in PE [33,53,54] and is due to the presence of short chain branching acting as point defects, which prevent large crystallites forming and hence gives low crystallinity. Lupolen 1840H has a significant amount of short and long chain branching, and appears to follow this trend, having a limited crystallite size.

Finally, Figure 10 graph D, shows that at constant height and increasing haul-off speed, the bulk crystallinity changes very little with an average value of ~20%, but it

does increase slightly down the tape-line, due to lamellae thickening as the tape cools. This low level of bulk crystallinity and the small crystalline layer thickness (H_b) are due to the chain branching defects present in the LDPE, as mentioned.

3.5 Crystallization processes in the extruded tape

From the SAXS data presented and the analysis performed we are in a position to discuss how the orientation and crystallization development occurs down the tape-line, in terms of the molecular chain extension processes involved. The molecular extension of polymer chains is described in terms of the coil-stretch transition during elongation flow proposed originally by de Gennes for dilute solutions [55]. This theory suggested that at a critical strain rate, polymer chains undergo a shape transition from a random coil configuration to a fully extended chain. Keller [4] went on to show how the coil-stretch transition could be applied to entangled polymer melts and was central in developing his well-known model of shish-kebab morphology. Here, the chain extension via flow or elongation processes, form the shish and at a later time the coiled chains then go on to form the crystalline outgrowths or kebabs [4,56]. This model is now widely accepted as the process by which crystallization in entangled polymer melts occurs under all types of flow.

During the extrusion process the entangled polymer chains will undergo some orientation or stretching in the extrusion barrel and die. However, the major chain stretching will be induced by the elongation al flow produced by the haul-off system once the polymer has left the die. The elongation process will orient and stretch the coiled chains, that is, once a critical strain rate is reached chains disentangle and are stretched out with the chain axis aligned in the direction of the tape-line (elongation direction). This results in the formation of the shish structures. The critical strain rate at a fixed temperature, is a function of the molecular weight distribution; higher molecular weight chains can be stretched at lower strain rates and lower molecular weight chains at much higher strain rates [15,56]. At constant strain rate a portion of molecules above the molecular weight threshold (M^*) will stretch fully, whereas chains below M^* will not stretch and remain as random coils. As the strain increases the molecular weight threshold M^*, decreases (more chains of lower molecular weight are stretched).

In our results at constant height, the orientation of the lamellae stacks increased with increasing haul-off speed up to ~28 m/min; this indicates that the higher effective strain rate in polymer tape converts more lower molecular weight chains in the amorphous regions into extended chains or shish. Thus, this causes an initial increase in the amorphous layer thickness (S_b) and hence long period L_p. As the shish become greater in density they provide increased nucleation points for the lower molecular weight coiled chains to then crystallize into the lamellae perpendicular to the oriented chains which manifests as equatorial scattering in the 2D SAXS patterns. At higher haul-off speeds (>28 m/min), the crystalline lamellae grow perpendicular to these shish and are restricted in their orientation so the 2D SAXS shows a meridional two-spot pattern representing a highly oriented regular lamellar morphology.

On travelling down the tape-line at constant haul-off speeds < 28 m/ min, the polymer material begins to cool and the insertion and thickening of the lamellae continues and therefore the L_p decreases (shown schematically in Figure 11). As the haul-off speed increases, the orientation of the lamellae stacks is almost at a maximum (begins to plateau as seen in the FWHM, Figure 7B) as does L_p and bulk crystallinity. Here, crystalline perfection of the lamellae stacks now appears to be the major process occurring and the 2D SAXS patterns shown as distinct two-spot patterns on the meridian confirm a regular stacked lamellar morphology. However, we have shown that molecular orientation persists at nil haul-off, that is, when the polymer tape is elongated under its own weight. The combination of the extrusion process and this elongation is still effective at stretching a portion of the polymer chains (high M_w) which act as shish. Under such weak orientation these shish are low in density (no equatorial scattering is seen) and are far apart. The kebabs nucleating from these shish grow and twist (like that seen in spherulitic growth) so a deviation in the orientations are seen from the perpendicular shish direction [34]. This process was observed in the 2D SAXS patterns (Figure 5) where on travelling down the tape-line, the meridional scattering displayed arcing indicating a shish-kebab type of structure which has a range of orientations around the elongation direction.

Finally, from the correlation function analysis, the bulk crystallinity remains relatively constant for LDPE and quite low (~20%), and is correlated with the H_b thickness being constant at ~ 50 Å, which is due to the significant short chain branching in this particular polymer. The short chain branching limits the crystalline lamellae thickness by acting as point defects (which are excluded from the growing crystal) and hence a low overall crystallinity attained.

4 Conclusions

During the extrusion and subsequent elongation of Lupolen LDPE tapes, the crystalline morphology and orientation was investigated as a function of processing parameters: extruder height and haul-off speed using SAXS. We have been able to control the haul-off speed directly and relate this to the applied stress in the polymer tape. The temperature and cross-sectional area of the tape was also measured at the point the X-ray data was collected. The tape temperature and cross-sectional area was seen to decrease with increasing haul-off speeds down the tape-line.

The haul-off speeds investigated in the tape extrusion process were relatively low (in comparison with melt-spinning), however significant orientation and crystalline morphology down the tape-line was observed. At lower haul-off speeds within our experimental parameters, orientation increased down the tape-line. The degree of orientation was seen to plateau at higher haul-off speeds as did the cross-sectional area and temperature. The crystalline morphology development down the tape-line at all haul-off speeds was consistent with a regular lamellar stack morphology, where the lamellae grow perpendicular to the elongation direction from highly extended molecular chains or shish. The concentration of shish increased with increasing haul-off speeds and at the highest haul-off speeds (highest density of shish) manifest as distinct scattering intensity on the equator at the same time as the meridional scattering from the lamellae stacks. The crystallization process down the tape-line was interpreted using the classical coil-stretch model for entangled polymer melts proposed by Keller [4].

At nil haul-off, the tape still had a significant amount of oriented shish present (from the extrusion and elongation process induced from the polymer weight itself) but

these were of low density and far apart allowing the twisting of the crystal kebabs as they grow resulting in a range of orientations around the elongation direction. In contrast from the highly oriented regular lamellar morphology when the tape is under constant haul-off, the final crystalline structure under nil haul-off conditions is described by a shish-kebab morphology.

Finally, due to the short-chain branching in the polymer, the final crystalline lamellae size and bulk crystallinity were relatively low under the processing conditions applied.

Acknowledgements

X-ray beam time at the ESRF was provided under the experimental application SC-1127 and ME-967. We are grateful for the assistance of all the ESRF DUBBLE-CRG beamline staff. Dr Yongfeng Men is acknowledged for assistance with experimental measurements using the Rheotens instrument kindly loaned by BASF, Germany.

References

[1] Wilkinson, A. N.; Ryan, A. J. '*Polymer Processing and Structure Development*', Kluwer, Dordrecht, 1998.

[2] Keller A.; Willmouth F. M., *J. Macromol. Sci*., 1972, B6, 493.

[3] Ward, I. M. '*Structure and properties of oriented polymers*' 1975, Wiley, New York.

[4] Keller, A., Kolnaar, H. W. '*Flow Induced Orientation and Structure Formation. In Processing of Polymers'*; Meijer, H. E. H., Ed.; 1997, VCH; New York, 187.

[5] Schultz, J. M., '*Polymer Crystallization. The Development of Crystalline Order in Thermoplastic Polymers*' Oxford, New York, 2001.

[6] Kornfield, J. A., Kumaraswamy, G., Issaian, A. M. *Ind. Eng. Chem. Res*. 2002, 41, 6383.

[7] Kumaraswamy, G., Kornfield, J. A., Yeh, F., Hsiao, B. S. *Macromols*. 2002, 35, 1762.

[8] Kumaraswamy, G., Verma, R. K., Kornfield, J. A., Yeh, F., Hsiao, B. S. *Macromols*. 2004, 37, 9005.

[9] Kumaraswamy, G. J. *Macromol. Sci., Part C: Polymer Reviews* 2005, 45, 375.

[10] Kanaya, T.; Polec, I. A.; Fujiwara, T.; Inoue, R.; Nishida, K.; Matsuura, T.; Ogawa, H.; Ohta, N. *Macromols*, 2013, 46, 3031.

[11] Shen, B.; Liang, Y.; Kornfield, J. A.; Han, C. H. *Macromols*, 2013, 46, 1528.

[12] Ren, Y.; Zha, L.; Ma, Y.; Hong, B.; Qiu, F.; Hu, W.; *Polymer*, 2009, 50, 5871.

[13] Mykhaylyk, O. O.; Chambon, P.; Impradice, C.; J. Patrick A. Fairclough, J. P. A.; Nick J. Terrill, M. J.; and Anthony J. Ryan . *Macromols*, 2010, *43*, 2389.

[14] Mykhaylyk, O. O.; Chambon, P.; Graham, R. S.; Fairclough, J. P. A.; Olmsted, P. D.; Ryan, A.J. *Macromols.*, 2008, *41*, 1901.

[15] Heeley, E. L., Fernyhough, C. M., Graham, R. S., Olmsted, P. D., Inkson, N. J., Embery, J, Groves, D. J., McLeish, T.C.B., Morgovan, A. C., Meneau, F., Bras, W. and Ryan, A. J. *Macromols.*, 2006; 39: 5058.

[16] Kimata, S.; Takashi Sakurai, T.; Nozue, Y.; Kasahara, T.; Yamaguchi, N.; Karino, Y.; Shibayama, M.; Kornfield, J. A. *Science*, 2007, 316, 1014-1017.

[17] Alig, I.; Steinhoff, B.; Lellinger, D. *Meas. Sci. Techno*., 2010, 21, 062001.

[18] Barnes, S.E.; Sibley, M. G.; Edwards, H. G. M.; Coates, P. D. *Trans. Inst. Meas. Control* 2007, 29, 453-465.

[19] Barnes, S.E.; Brown, E. C., Sibley, M. G.; Edwards, H. G. M.; Scowen, I. J.; Coates, P. D. *Appl. Spectrosc*. 2005, 59, 611-619,.

[20] Bras, W.; Ryan, A. J.. *J. Appl. Cryst.*, 1997, 30, 816-821.

[21] Cakmak, M.; Teitge, A.; Zachmann, H. G.; White, J. L. *J. Polym.Sci. Part B: Polym. Phys*., 1993, 31, 371.

[22] Ryan, A. J.; Elwel, M. J.; Bras, W. *Nucl. Instrm. Methods Phys. Res. B.* 1995, 97, 216.

[23] Rybnikar, F.; Kaszonyiova, M.; Cermak, R.; Habrova, V.; Obadal, M. *J. Appl. Polym. Sci.* 2013, 128, 1665.

[24] Zheng, G.; Jia, Z.; Li, S.; Dai, K.; Liu, B.; Zhang, X.; Mi, L.; Liu, C.; Chen, J.; Shen, C.; Peng, X.; Li, Q. *Polym. Int.* 2011, 60, 1434.

[25] Murase, H.; Ohta, Y.; Hashimoto, T. *Macromols.* 2011, 44, 7335.

[26] Polaskova, M.; Cermak,; Sedlacek, T.; Kalus, J.; Obadal, M.; Saha, P. *Polym. Compos*. 2010, 31: 1427.

[27] Chen, P.; Afshari, M.; Cuculo, J. A.; Kotek, R. *Macromols*. 2009, 42, 5437.

[28] Hirahata, H.; Seifert, S.; Zachmann, H. G.; Yabuki, K. *Polymer* 1996, 37 5131.

[29] Terrill, N. J. Fairclough, P. A.; Towns-Andrews, E.; Komanschek, B. U.; Young, R. J.; Ryan, A. J. *Polymer*, 1998, 39, 2381.

[30] Heeley, E.L.; Poh, C.K.; Li, W.; Maidens, A.; Bras, W.; Dolbnya, I.P.; Gleeson, A.J.; Terrill, N.J. ; Fairclough, J. P.A.; Olmsted, P.D.; Ristic, R.I.; Hounslow M. J.; Ryan, A.J. *Faraday Discuss*. 2003, 122, 343.

[31] Heeley; E.L.; Gough, T.; Bras, W.; Gleeson, A.J.; Coates, P.D.; Ryan , A.J. *Nucl. Instr. Meth. Phys. Res. B*. 2005, 238, 21.

[32] Bras, W.; Dolbnya, I. P.; Detollenaere, D.; van Tol, R.; Malfois, M.; Greaves, G. N. Ryan A. J.; Heeley, E. *J. Appl. Cryst*. 2003**,** 36, 791.

[33] Heeley, E. L.; Maidens, A. V.; Olmsted, P. D.; Bras, W.; Dolbnya, I. P.; Fairclough, J. P. A.; Terrill, N. J.; Ryan, A. J.; *Macromols*., 2003, 36, 3656.

[34] Samon, J.M.; Schultz, J. M.; Hsiao, B. S.; Seifert, S.; Stribeck, N.; Gurke, I.; Collins, G.; Saw, C. *Macromols.* 1999, 32, 8121.

[35] Samon, J. M.; Schultz, J. M.; Wu, J.; Hsiao B. S.; Yeh, F.; Kolb, R.; *J. Polym Sci: B Polym Phys.* 1999, 37,1277.

[36] Schultz, J. M.; Hsiao, B. Samon, J. M.; *Polymer* 2000, 41, 8887.

[37] Samon, J. M.; Schultz, J. M.; Hsiao, B. S. *Polymer* 2002;43, 1873.

[38] Samon, J. M.; Schultz, J. M.; Hsiao, B. S.; Khot, S.; Johnson, H. R. *Polymer* 2001, 42, 1547.

[39] Kolb, R.; Seifert S, Stribeck N, Zachmann HG. *Polymer* 2000, 41, 1497.

[40] Wagner, M. H.; Schulze, V.; Göttfert, A. *Polym. Eng. Sci.* 1996; 36, 625.

[41] Sentmanat, M.; Wang, B.N.; McKinley, G. H.; *J. Rheol*. 2005, 49, 585.

[42] http://www.small-angle.ac.uk/small-angle/Software.html.

[43] Ryan, A. J. *Fibre Diffrac. Rev.*1994, 3, 25.

[44] Porod. G. *Kolloid Z*. 1951, 124, 83.

[45] Baltá-Calleja, F. J., Vonk, G. G. *X-ray Scattering of Synthetic Polymers*. Elsevier Science, New York, 1989.

[46] Strobl, G. R., Schneider, M. *J. Polym. Sci. Polym. Phys. Edn.* 1980, 18, 1343.

[47] Strobl, G. R., Schneider, M., Voigt-Martin, I. G. *J. Polym. Sci. Polym. Phys. Edn.* 1980, 18, 1361.

[48] Wang, Z-G.; Hsiao, B. S.; Murthy, N. S.; *J. Appl. Cryst*. 2000, 33, 690.

[49] Carmarillo, A. A.; Stribeck, N. *Fibres and Textile in Eastern Europe*, 2005, 13, 27.

[50] Jiang, Z.; Tang, Y.; Rieger, J.; Enderle, H-F.; Lilge, D.; Roth, S. V.; Gehrke, R.; Wu, Z.; Li, Z., Li, X.; Men, Y. *Eur. Polym. J*., 2010, 46, 1866.

[51] Rober S., Bosecke, P., Zachmann, H. G. *Makromol. Chem., Macromol. Symp*. 1988, 15, 295.

[52] Stribeck, N. *J. Polym. Sci. B: Polym. Phys.* 1999, 37, 975.

[53] Ryan, A. J., Hamley, I. W., Bras, W., Bates, F. S. *Macromols*. 1995, 28, 3860.

[54] Hamley, I.W., Fairclough, J. P. A., Bates F. S., Ryan A. J. *Polymer*, 1998**,** 39 1429.

[55] de Gennes, P. G. *J. Phys., Chem*., 1974, 15, 60.

[56] Somani, R. H., Yang, L., Zhu, L., Hsiao, B. S. *Polymer*, 2005, 46, 8587.